Estimation of Newtonian noise from the KAGRA cooling system

Rishabh Bajpai[*]

*The Graduate University for Advanced Studies, Department of Accelerator Science, School of High Energy
Accelerator Science, High Energy Accelerator Research Organization (KEK) Tsukuba,
Ibaraki 305-0801, Japan*

Takayuki Tomaru

*National Astronomical Observatory of Japan, 2-21-1 Osawa, Mitaka, Tokyo 181-8588, Japan;
The University of Tokyo, Department of Astronomy, Graduate School of Science,
2-21-1 Osawa, Mitaka, Tokyo 181-8588, Japan;
The Graduate University for Advanced Studies, 2-21-1 Osawa, Mitaka, Tokyo 181-8588, Japan
and High Energy Accelerator Research Organisation, 1-1 Oho, Tsukuba, Ibaraki 305-0801, Japan*

Toshikazu Suzuki

*Institute for Cosmic Ray Research (ICRR), The University of Tokyo,
5-1-5, Kashiwanoha, Kashiwa, Chiba 277–8582, Japan*

Kazuhiro Yamamoto

Department of Physics, University of Toyama, Toyama, Toyama 930-8555, Japan

Takafumi Ushiba

*The University of Tokyo Institute for Cosmic Ray Research Kamioka Observatory,
Higashimozumi 238, Kamioka, Hida, Gifu 506-1205, Japan*

Tohru Honda

High Energy Accelerator Research Organisation, 1-1 Oho, Tsukuba, Ibaraki 305-0801, Japan

KAGRA is the first kilometer scale gravitational wave detector to be constructed underground and employ cryogenics to cool down its test masses. While the underground location provides a quiet site with low seismic noise, the cooling infrastructure is known to generate large mechanical vibrations due to cryocooler operation and structural resonances of the cryostat. As cooling system components are relatively heavy and in close proximity to the test masses, oscillation of gravity force induced by their vibration, so-called Newtonian noise, could contaminate the detector sensitivity. In this paper, we use the results from vibration analysis of the KAGRA cryostat to estimate cooling system Newtonian noise in the 1–100 Hz frequency band. Our calculations show that, while this noise does not limit the current detector sensitivity or inspiral range, it will be an issue in the future when KAGRA improves its sensitivity. We conclude that KAGRA may need to implement Wiener filters to subtract this noise in the future.

I. INTRODUCTION

Ground-based gravitational wave (GW) detectors are ultrasensitive laser interferometers that detect displacements of the order of 10^{-19} m between mirrors several kilometers apart, making it essential to minimize environmental displacement noise. Seismic noise (ground motion) is one of the fundamental noise sources for second-generation GW detectors like KAGRA [1,2], LIGO [3], and Virgo [4]. It couples to the test masses in two ways: (a) direct mechanical coupling, and (b) Newtonian noise (NN). While, the mechanical coupling of seismic noise can be well attenuated by suspending the test masses from highly efficient vibration isolation systems [5,6], Newtonian noise cannot be shielded against.

Newtonian noise is caused by fluctuation of local gravitational fields caused by fluctuating mass distributions around test masses. Over the past few decades, several studies have been conducted to evaluate the NN from seismic fields, vibrating objects, and atmospheric fields [7–11], but their contribution as noise sources are limited to

[*]bajpai@post.kek.jp

the low frequency outside the sensitivity band for second-generation detectors. However, Newtonian noise will be a serious issue for third-generation detectors like the Einstein Telescope [12] and the Cosmic Explorer [13]. The Einstein Telescope aims to push the low-frequency sensitivity of ground-based GW detectors to its limit by increasing the arm length, using cryogenics to cool down the test masses and constructing detectors underground.

The large-scale cryogenic gravitational wave telescope (KAGRA), is a dual recycled Fabry-Perot Michelson interferometer-based GW detector located in Gifu, Japan. Compared to other second-generation detectors it has two unique features; first, the detector is located underground, which provides a quiet site (low seismic noise) and second, the mirrors are cooled down to 20 K reducing the thermal noises. It is these features that make KAGRA an ideal testbed for the development of the third-generation detectors.

While some studies have been conducted at the KAGRA site to evaluate the seismic and atmospheric NN [14] and underground water NN [15], NN contribution from the KAGRA cooling system [16] has not been evaluated. Vibration analysis of the cryostat at cryogenic temperature [17] showed that vibration of the cooling system components surrounding the test masses is 2–3 orders larger than the seismic motion in the 1–100 Hz band due to structural resonances and cryocooler operation. As these components are relatively heavy and in close proximity to the test mass, their NN contribution could contaminate the detector sensitivity. A similar study for the LIGO vacuum chamber was conducted [9] and concluded that NN from the chamber did not contaminate the detector sensitivity.

In a recent study, LIGO estimated the Newtonian noise coupling from the cryogenic shield being developed for radiative cooling in next-generation LIGO observatories [18]. In this paper, we present methods, considerations, calculations, and results of Newtonian noise from the KAGRA cooling system using the vibration spectra measured at 12 K. We hope our study can serve as a guide in designing the cryogenic infrastructure of third-generation detectors.

II. THEORY

A. Derivation of expression for Newtonian noise

To derive the expression for Newtonian noise, we consider a simple hollow cuboid-shaped cooling system with the test mass (TM) (sapphire mirror of mass $M = 23$ kg) as a point mass located at the origin, as shown in Fig. 1(a). The entire cuboid cooling system is considered as a mass distribution made up of N point masses (finite elements), each weighing m_n and denoted by gray squares. For a mass m_n at a position $\vec{r}_n(x_n, y_n, z_n)$ on the cooling system, the Newtonian force on TM is
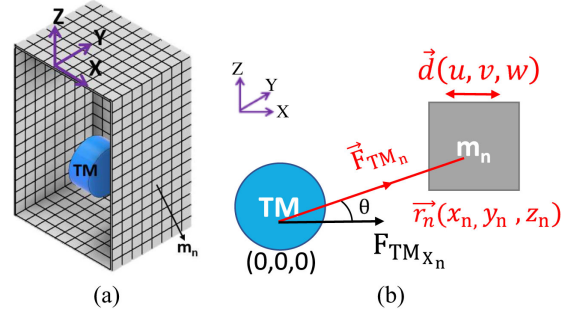

FIG. 1. (a) A simple hollow cuboid cooling system TM configuration is considered to derive the Newtonian noise expression. The TM is located at the origin, and the cuboid is split into N elements each weighing m_n and denoted by the gray squares. (b) Newtonian force on TM due to a single element on the cooling system at position $\vec{r}(x_n, y_n, z_n)$ is $\vec{F}_{TM}$. The mass is being displaced (vibrating) by a small amount $\vec{d}(u, v, w)$, such that $|r| \gg |d|$. The coordinate system considered is shown with purple arrows and the x-axis is parallel to the optical axis.

$$\vec{F}_{TM_n} = GMm_n \frac{\vec{r}}{|\vec{r}|^3}, \tag{1}$$

where G is the gravitational constant. Figure 1(b) shows this system. Now, the x-component of this force (along the optical axis of the interferometer) is

$$F_{TM_{X_n}} = GMm_n \frac{x_n}{(x_n^2 + y_n^2 + z_n^2)^{\frac{3}{2}}}. \tag{2}$$

The gradient of this expression is

$$\nabla F_{TM_{X_n}} = \frac{\partial F_{TM_{X_n}}}{\partial x_n} \hat{i} + \frac{\partial F_{TM_{X_n}}}{\partial y_n} \hat{j} + \frac{\partial F_{TM_{X_n}}}{\partial z_n} \hat{k}$$

$$= GMm_n \left[\frac{(-2x_n^2 + y_n^2 + z_n^2)\hat{i} - 3x_n y_n \hat{j} - 3z_n x_n \hat{k}}{(x_n^2 + y_n^2 + z_n^2)^{\frac{5}{2}}} \right], \tag{3}$$

where $\hat{i}$, $\hat{j}$, and $\hat{k}$ are unit vectors along the x, y, and z axes, respectively.

If mass m_n moves/vibrates by a small amount $\vec{d}$,

$$\vec{d} = u(t)\hat{i} + v(t)\hat{j} + w(t)\hat{k}. \tag{4}$$

The change in force on test mass along the x-axis due to displacement $\vec{d}$ is the scalar product $\nabla F_{TM_{X_n}} \cdot \vec{d}$, which gives us

$$\delta F_{TM_{X_n}}(t)$$
$$= GMm_n \left[\frac{(-2x_n^2 + y_n^2 + z_n^2)u(t) - 3x_n y_n v(t) - 3z_n x_n w(t)}{(x_n^2 + y_n^2 + z_n^2)^{\frac{5}{2}}} \right]. \tag{5}$$

Ignoring the internal resonances of the cooling system, it is assumed that each element moves with the same displacement. So the change in force on the TM due to the entire cooling system (CS) will be

$$\delta F_{\text{TM}_{X_{CS}}}(t) = GM[Au(t) + Bv(t) + Cw(t)], \quad (6)$$

where $A = \sum_{n=1}^{N} m_n \left[\frac{-2x_n^2 + y_n^2 + z_n^2}{(x_n^2 + y_n^2 + z_n^2)^{\frac{5}{2}}} \right]$, $B = \sum_{n=1}^{N} m_n \left[\frac{-3x_n y_n}{(x_n^2 + y_n^2 + z_n^2)^{\frac{5}{2}}} \right]$, $C = \sum_{n=1}^{N} m_n \left[\frac{-3z_n x_n}{(x_n^2 + y_n^2 + z_n^2)^{\frac{5}{2}}} \right]$, are constants. Now, the Fourier transform of Eq. (6) is

$$\delta F_{\text{TM}_{X_{CS}}}(\omega) = GM[Au(\omega) + Bv(\omega) + Cw(\omega)], \quad (7)$$

where ω is the angular frequency.

The power spectral density of an ergodic signal $P(t)$ is defined as $\langle P(\omega)P^*(\omega') \rangle = S_P(\omega)\delta(\omega - \omega')$, the amplitude spectral density of $\delta F_{\text{TM}_{X_{CS}}}(t)$, $\sqrt{S_{F_{\text{TM}_{X_{CS}}}}(\omega)}$ will be

$$\sqrt{S_{F_{\text{TM}_{X_{CS}}}}(\omega)} = GM\sqrt{A^2 S_u(\omega) + B^2 S_v(\omega) + C^2 S_w(\omega)}, \quad (8)$$

where $S_u(\omega), S_v(\omega),$ and $S_w(\omega)$ are power spectral densities of the cooling system vibration along x, y, and z axes and it is assumed they have no correlation between them.

Now Eq. (8) gives us the amplitude spectral density of force fluctuation and dividing it by $1/M\omega^2$ gives us displacement spectral density for one test mass. Since, similar vibration coupling with no correlation for all four test masses is expected, a factor of $\sqrt{4}$ is multiplied. Finally dividing the expression with detector arm length, L ($= 3000$ m) gives us the corresponding strain amplitude of cooling system Newtonian noise as

$$\sqrt{S_h(\omega)} = \frac{\sqrt{4}G}{\omega^2 L} \sqrt{A^2 S_u(\omega) + B^2 S_v(\omega) + C^2 S_w(\omega)} \equiv H. \quad (9)$$

B. Considerations for the KAGRA cooling system

In KAGRA the 23 kg sapphire test masses are suspended from a nine-stage vibration isolation system and cooled down inside a double radiation shield cryostat [16]. Figure 2 shows the cross section of the KAGRA cryostat and components (chamber, baffle, breadboard, inner, and outer radiation shield) considered for Newtonian noise calculation are denoted with red boxes. The mirror is considered to be a point mass at the origin. The coordinate system for the NN calculation is denoted by the blue arrows as

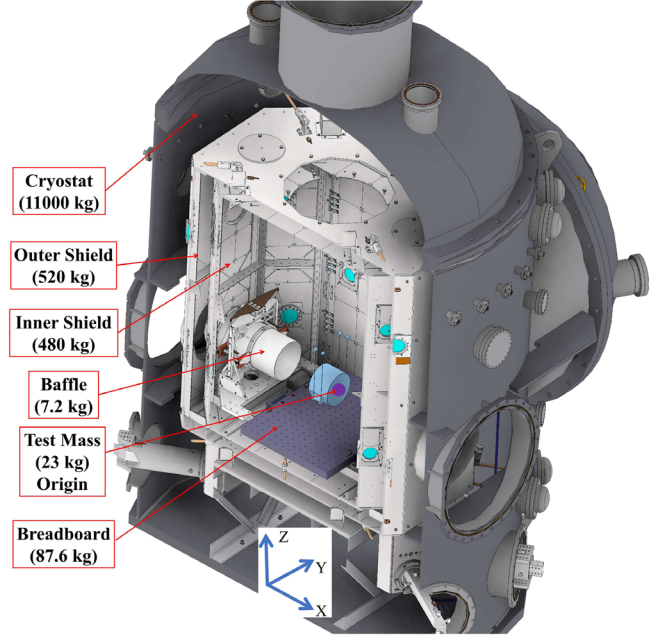(i) *x-axis* is the optical axis of the interferometer,

FIG. 2. Coordinate system and summary of components considered in the Newtonian noise calculation. Cross section of KAGRA cryostat showing the components (chamber, baffle, breadboard, inner shield, and outer shield) considered for the Newtonian noise calculation. The blue arrows denote the coordinate system. The test mass is considered as a point mass, located at origin as denoted by the purple dot.

(ii) *y-axis:* is the horizontal axis perpendicular to the optical axis,

(iii) *z-axis:* is the vertical axis.

The expression derived in Eq. (9) gives the Newtonian noise strain for a simple mass distribution/test mass configuration; for the KAGRA cooling system the mass distribution is much more complex. Newtonian noise is evaluated by generating a mesh with N elements in Ansys Mechanical Enterprise (software based on finite-element method) and solving it for Eq. (9). Table I shows the values of A, B, and C as evaluated from the mesh generated for each component.

Since A is dominant value, we only consider the effect of vibration along the *x*-axis (optical axis) to estimate the Newtonian noise coupling of each component. Then Eq. (9) is then reduced to

TABLE I. The values of the summations A, B, and C of various components for the generated mesh. The units are kg/m^3.

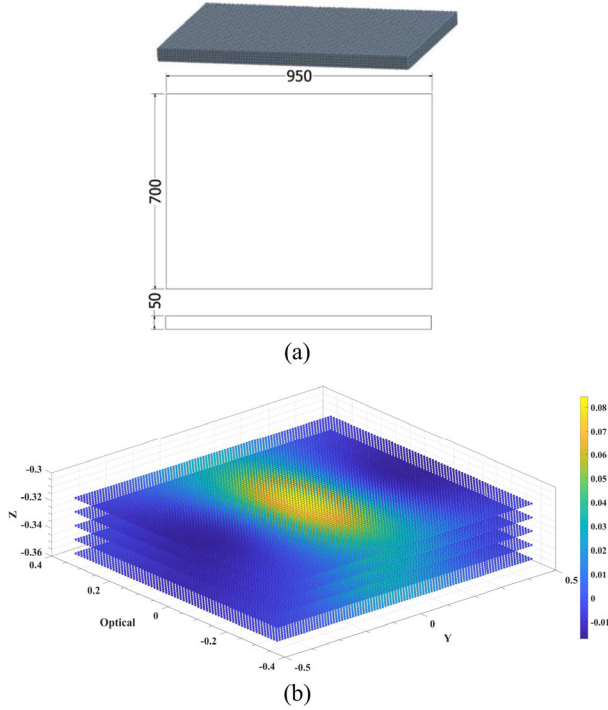| Component	A	B	C
Breadboard	550.69	-5.4×10^{-16}	-1.2×10^{-14}
Baffle	-23.4	-6.97	-0.11
Inner shield	124.15	-0.28	-4.64
Outer shield	97.52	0.53	-1.95
Cryostat	-298.34	-6.22	-0.03

(a)

(b)

FIG. 3. (a) Mesh generated and 2D drawing for the breadboard. The cuboid is divided into 33,250 elements each weighing 2.634 g. (b) 3D scatter plot where each dot represents an element n from breadboard mesh while the color is value $S_{n_{\text{breadboard}}}$ of that element in Eq. (11).

$$H_{\text{NN}} = \frac{\sqrt{4}G}{\omega^2 L} \times \sqrt{S_u(\omega)} \times A$$

$$= \frac{K}{\omega^2} \times u_{\text{component}} \sum_{n=1}^{N} S_{n_{\text{component}}}, \qquad (10)$$

where $K = \frac{\sqrt{4}G}{L} = 4.44 \times 10^{-14}$ m^2 kg^{-1} s^{-2}, $S_{n_{\text{component}}} = [m_n(\frac{(-2x_n^2+y_n^2+z_n^2)}{(x_n^2+y_n^2+z_n^2)^{\frac{5}{2}}})]$ kg/m^3, and $u_{\text{component}} = \sqrt{S_u(\omega)}$, is displacement spectral density of vibration (in m/$\sqrt{\text{Hz}}$) of the component under consideration.

III. CALCULATION

A. Breadboard

The breadboard is an aluminum cuboid plate of dimension $0.7 \times 0.95 \times 0.05$ m and mass of 87.6 kg at a distance of 0.335 m from the TM. The board is bolted to the bottom of the inner shield and is used to fix the earthquake stop frame for the cryogenic payload [19]. The generated mesh had elements size of 0.01 m splitting cuboid into 33,250 elements, each weighing 2.634 g. Figure 3(a) shows the generated mesh and 2D drawing of breadboard. Based on the generated mesh Eq. (10) becomes

$$H_{\text{breadboard}} = \frac{K}{\omega^2} \times u_{\text{breadboard}} \sum_{n=1}^{33250} S_{n_{\text{breadboard}}}. \qquad (11)$$
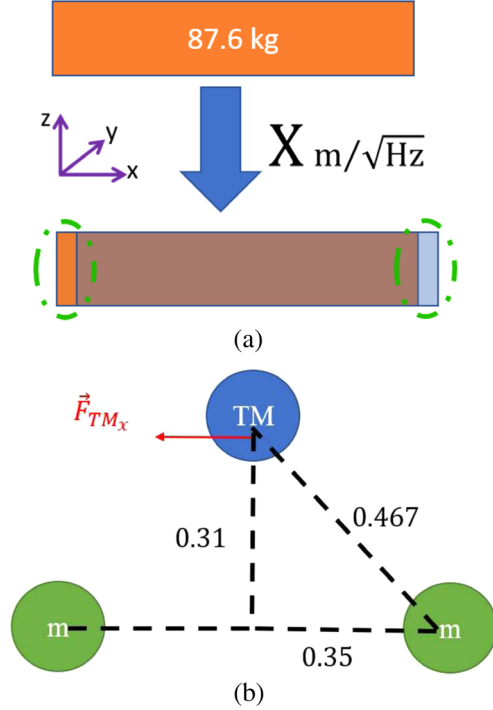

(a)

(b)

FIG. 4. (a) Front view of the breadboard, being displaced X m/$\sqrt{\text{Hz}}$. The dotted green circle represent mass that causes gravity fluctuations. (b) A simple point mass representation of Fig. 4(a) showing relative position of test mass and breadboard point masses m.

The value of summation $\sum_{n=1}^{33250} S_{n_{\text{breadboard}}}$ is 550.697 kg/m^3, substituting the values in Eq. (11) we get

$$H_{\text{breadboard}} = 2.295 \times 10^{-11} \times \frac{u_{\text{breadboard}}}{\omega^2}, \qquad (12)$$

where $u_{\text{breadboard}}$ is the vibration (displacement) measured [17] at 12 K.

A simplified system, shown in Fig. 4, was considered to confirm the simulation result. Figure 4(a) shows the front view of the breadboard. Now, if the displacement (vibration) spectra of the breadboard is X m/$\sqrt{\text{Hz}}$ at some frequency f. The force acting on the TM will only be due to the small mass, represented by green dotted circles [in Fig. 4(a)] displaced at the ends of the breadboard. A simplified representation of this is shown in Fig. 4(b), from which the force on TM along x-axis can be calculated as

$$\vec{F}_{TM_{X_{\text{breadboard}}}} = 2.G.M.m.\frac{0.35}{0.467^3}, \qquad (13)$$

where m is 87.6X kg at some frequency f and M is the mass of the test mass from Eq. (13) the expression for strain can be derived as

$$H_{\text{breadboard}} = \frac{\sqrt{4}}{\omega^2.L} \times 2 \times G \times 87.6X \times 3.436, \qquad (14)$$

where $X = u_{\text{bottom}}$ is the vibration measured by the cryogenic accelerometer,

$$H_{\text{breadboard}} = 2.676 \times 10^{-11} \times \frac{u_{\text{bottom}}}{\omega^2}. \qquad (15)$$

Comparing Eqs. (12) and (15) it is clear that results NN coupling from breadboard, calculated by computer simulation and by hand are comparable and there is no significant error.

B. Baffle

The wide-angle baffle (WAB) is a hollow cylinder suspended 10 mm in front of the high reflectivity (HR) side of each TM to prevent the backscattered light from recoupling to the main beam as it is coated in SolBlack. The cylinder is 570 mm long with an inner diameter of 254 mm; it is 4 mm thick and is made of aluminum weighing about 2 kg. The total suspended mass is about 7.2 kg and the natural frequency of the longitudinal mode is about 0.84 Hz. A detailed review of WAB can be found at [20,21].

Note that for the calculations, the entire 7.2 kg mass was assumed to be evenly distributed across the cylinder. The generated mesh had elements size of 0.004 m splitting the cylinder into 29,601 elements, each weighing 0.24 g. Figure 5(a) shows the generated mesh and 2D drawing of the baffle. Based on the generated mesh Eq. (10) becomes

$$H_{\text{baffle}} = \frac{K}{\omega^2} \times u_{\text{baffle}} \sum_{n=1}^{29601} S_{n_{\text{baffle}}}. \qquad (16)$$

The value of summation $\sum_{n=1}^{29601} S_{n_{\text{baffle}}}$ is -24.75 kg/m³, substituting the values in Eq. (16) we get

$$H_{\text{baffle}} = -9.76 \times 10^{-13} \times \frac{u_{\text{baffle}}}{\omega^2}, \qquad (17)$$

where $u_{\text{baffle}} = u_{\text{breadboard}} \times$ transfer function of the baffle suspension

The baffle suspension is rigidly bolted to the breadboard and since the longitudinal mode of the suspended baffle is 0.84 Hz, the transfer function is $\frac{0.84^2}{f^2}$ for $f > 0.84$ Hz, where f is the frequency. Therefore, Eq. (17) becomes

$$H_{\text{baffle}} = -6.88 \times 10^{-13} \times \frac{u_{\text{breadboard}}}{\omega^2 f^2}. \qquad (18)$$

C. Thermal radiation shield

Test masses are cooled down inside a double thermal radiation shield, which are octagonal prism structures with a combined weight of ~1000 kg. These shields, made of aluminum (Al1070) are called inner/8 K and outer/80 K shield, weighing ~480 kg and ~520 kg, respectively. As can be seen in Fig. 2, the shield structure is relatively complex including multiple components (like support beams, view ports, screws, etc.), to simplify the calculation
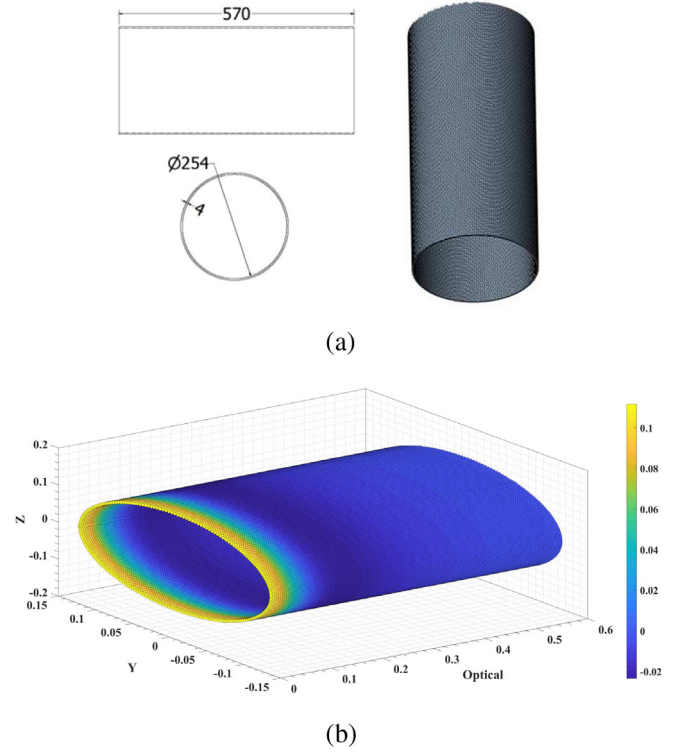

(a)

(b)

FIG. 5. (a) Mesh generated for baffle. The cylinder is divided into 29,601 elements each weighing 0.24 g. (b) 3D scatter plot where each dot represents an element n from baffle mesh while the color is value $S_{n_{\text{baffle}}}$ of that element in Eq. (16).

we considered a simple octagonal prism with the same dimensions as the shields. The generated mesh and dimension of each shield can be found in Figs. 6(a) and 7(a).
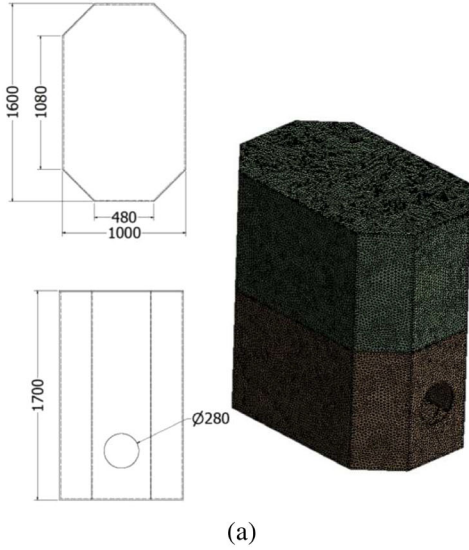
1. 8 K shield

Figure 6(a) shows the generated mesh for a simplified inner (8 K) shield, based on which the expression for Eq. (10) becomes

$$H_{\text{8K}} = \frac{K}{\omega^2} \times u_{\text{8K}} \sum_{n=1}^{200935} S_{n_{\text{8K}}}. \qquad (19)$$

In Eq. (19) u_{8K} is the vibration (displacement) of inner shield; due internal resonances of chamber and shield the magnitude of vibration will increase as we move along the z-axis. Vibration of elements on the top ($u_{\text{8K}_{\text{top}}}$) and bottom ($u_{\text{8K}_{\text{bottom}}}$) surfaces will be constant while that of the walls will be a function of z ($u_{\text{8K}_{\text{walls}}}(z)$).

To precisely estimate the NN coupling we need to evaluate the displacement of wall elements for each resonance mode; as the computing resources were limited we split the shield into two equal halves and assume that the top and bottom section move with $u_{\text{8K}_{\text{top}}}$ and $u_{\text{8K}_{\text{bottom}}}$, respectively. From this, Eq. (19) can be simplified to
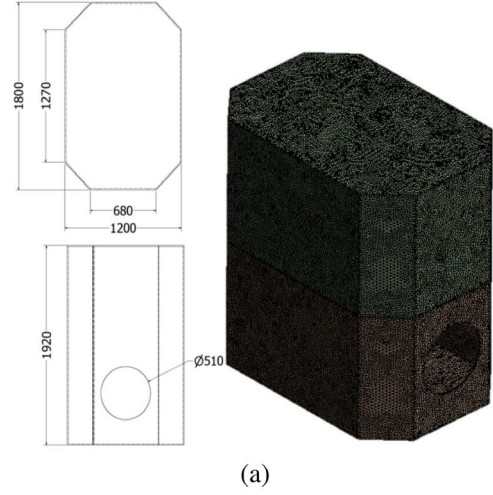
(a)
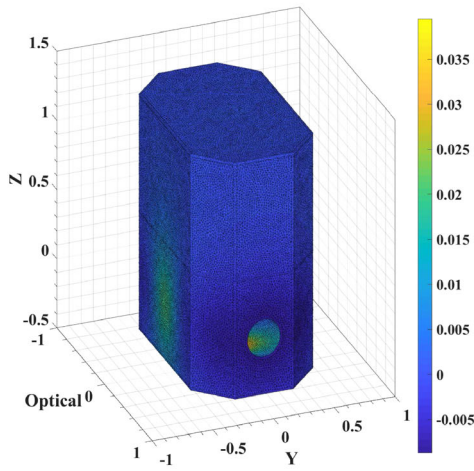
(b)

FIG. 6. (a) Mesh generated for inner shield with 200,935 elements each weighing 2.4 g. 2D drawing showing top and front view of 8 K shield. (b) 3D scatter plot where each dot represents an element n from inner-shield mesh while the color is value $S_{n_{8K}}$ of element in Eq. (19).
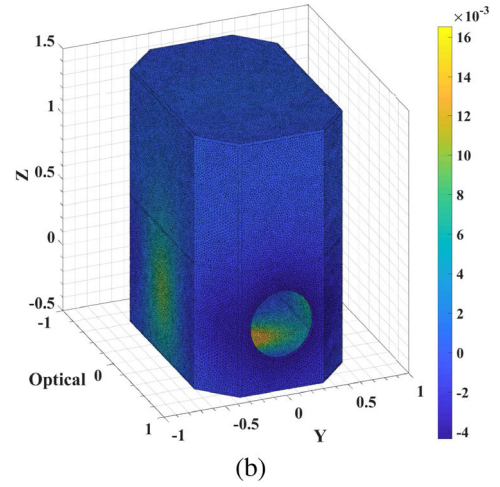
$$H_{8K} = \frac{K}{\omega^2} \times \left[u_{8K_{bottom}} \sum_{n=1}^{99882} S_{n_{8K_{bottom}}} \right.$$

$$\left. + u_{8K_{top}} \sum_{n=99883}^{200935} S_{n_{8K_{top}}} \right]. \tag{20}$$

The value of summation $\sum_{n=1}^{99882} S_{n_{8K_{bottom}}}$ and $\sum_{n=99883}^{200935} S_{n_{8K_{top}}}$ is 59.5 kg/m³ and 6.466 kg/m³, respectively. Substituting these values in Eq. (20) we get

$$H_{8K} = 2.48 \times 10^{-12} \times \frac{u_{8K_{bottom}}}{\omega^2} + 2.69 \times 10^{-12} \times \frac{u_{8K_{top}}}{\omega^2}. \tag{21}$$

(a)

(b)

FIG. 7. (a) Mesh generated for outer shield with 262,889 elements each weighing 1.97 g. 2D drawing showing top and front view of 80 K shields. (b) 3D scatter plot where each dot represents an element n from outer-shield mesh while the color is value $S_{n_{80K}}$ of that element in Eq. (22).

2. 80 K shield

Figure 7(a) shows the generated mesh for a simplified outer (80 K) shield, based on which the expression for Eq. (10) becomes

$$H_{80K} = \frac{K}{\omega^2} \times u_{80K} \sum_{n=1}^{262899} S_{n_{80K}}. \tag{22}$$

To calculate the NN noise from the 80K shield we make the same considerations as the 8 K shield. As it was difficult to practically measure the 80 K shield vibration, we assume it to be same as that of the 8 K shield. The 80K shield was also split into two equal halves; the generated mesh had 262,899 elements each weighing 1.97 gm. Based on the generated mesh, Eq. (22) becomes

$$H_{80K} = 2.34 \times 10^{-12} \times \frac{u_{80K_{bottom}}}{\omega^2} + 1.73 \times 10^{-12} \times \frac{u_{80K_{top}}}{\omega^2},$$
(23)

where $u_{80K_{bottom}} = u_{8K_{bottom}}$ and $u_{80K_{top}} = u_{8K_{top}}$ is assumed.

D. Cryostat chamber

The cryostat chamber (height: 4.33 m, outer diameter: 2.3 m) is a stainless steel structure (SUS-304) weighing about 11,000 kg. The structure itself has various flanges which we ignore in our calculation and consider a simple structure, shown in Fig. 8(a) along with the mesh. Based on the generated mesh the expression for Eq. (10) becomes
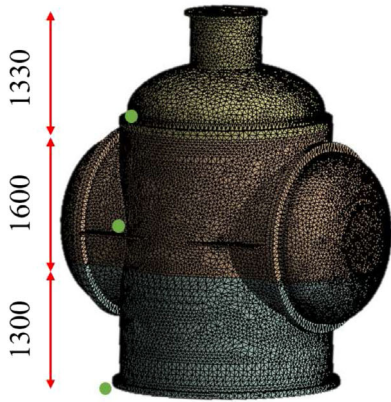
(a)
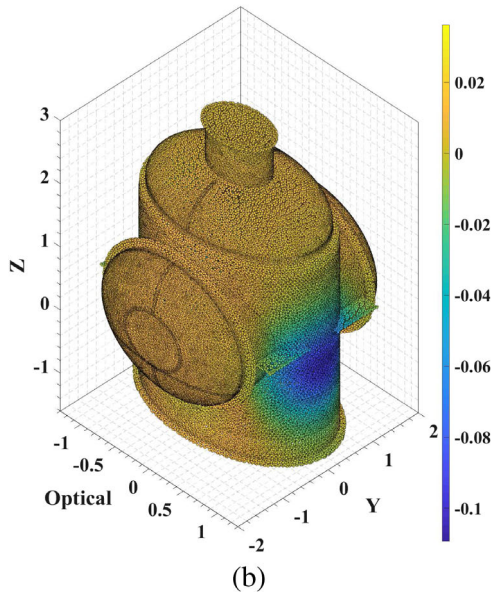
(b)

FIG. 8. (a) Mesh generated for cryostat with 124,795 elements. Cryostat was split into three parts and the green dots represent the position where vibrations u_{top}, u_{middle} and u_{bottom} were measured. (b) 3D scatter plot where each dot represents an element n from cryostat mesh while the color is value $S_{n_{cryostat}}$ of that element in Eq. (24).

$$H_{cryostat} = \frac{K}{\omega^2} \times u_{cryostat} \sum_{n=1}^{124795} S_{n_{cryostat}}.$$
(24)

To evaluate NN from the cryostat we divide it into three sections: top, middle, and bottom with vibrations u_{top}, u_{middle}, and u_{bottom}, respectively. The expression in Eq. (24) becomes

$$H_{cryostat} = \frac{K}{\omega^2} \times \left[u_{top} \sum_{n=1}^{18908} S_{n_{top}} + u_{middle} \sum_{n=60254}^{124795} S_{n_{middle}} \right.$$
$$\left. + u_{bottom} \sum_{n=18909}^{60253} S_{n_{bottom}} \right].$$
(25)

The value of the summations $\sum_{n=1}^{18908} S_{n_{top}}$, $\sum_{n=60254}^{124795} S_{n_{middle}}$, and $\sum_{n=18909}^{60253} S_{n_{bottom}}$ are 101.99 kg/m^3, -317.9 kg/m^3, and -82.43 kg/m^3, respectively. Substituting these values in Eq. (25) we get

$$H_{cryostat} = 6.8 \times 10^{-9} \times \frac{u_{top}}{\omega^2} - 2.12 \times 10^{-8} \times \frac{u_{middle}}{\omega^2}$$
$$- 5.49 \times 10^{-9} \times \frac{u_{bottom}}{\omega^2}.$$
(26)

E. Vibration spectra

Figure 9 shows the vibration spectra of each component and the measurement conditions are mentioned below:

(i) The breadboard vibration ($u_{breadboard}$) shown above was measured at 12 K using a cryogenic accelerometer [22] in [17].

(ii) As the breadboard is rigidly bolted to the bottom of the inner/8 K shield, the vibration of shield bottom ($u_{8K_{bottom}}$) will be same as that of breadboard.

(iii) The vibration of top of the inner shield ($u_{8K_{top}}$) was calculated as the product of breadboard vibration at 12 K and vibration coupling from bottom to top of the shield, measured at room temperature using a commercial accelerometer (*TOKKYOKIKI MG-102S*).
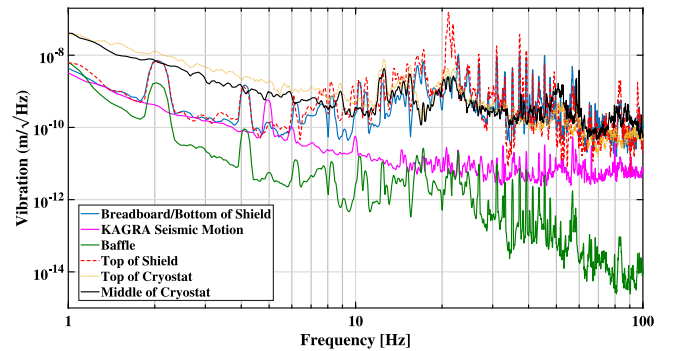

FIG. 9. Vibration spectra of various components considered during Newtonian noise estimation.
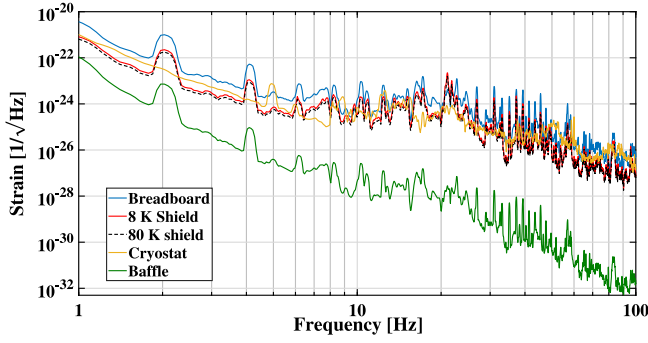
FIG. 10. Comparison of Newtonian noise strain spectral density from each component, the largest contribution comes from breadboard followed by radiation shields, cryostat, and baffle. Note that the force on the test mass due breadboard/radiation shields and cryostat/baffle are in opposite directions.

(iv) For the outer/80K shield $u_{80K_{bottom}} = u_{8K_{bottom}}$ and $u_{80K_{top}} = u_{8K_{top}}$ is assumed.

(v) The baffle suspension is rigidly bolted to the breadboard so its vibration (u_{baffle}) is the product of breadboard vibration ($u_{breadboard}$) and suspension transfer function. Since the longitudinal mode of the suspended baffle is 0.84 Hz, the transfer function is $\frac{0.84^2}{f^2}$ for $f > 0.84$ Hz.

(vi) The cryostat was divided into three parts, while the top and middle vibrations (u_{top} and u_{middle}, respectively) were measured by *TOKKYOKIKI MG-102S*, the bottom vibration (u_{bottom}) is same as KAGRA seismic motion and measured using *RION LA-50*.

F. Comparison

Substituting the measured vibration of each component (Fig. 9) in Eqs. (12), (18), (21), (23), and (26) we get the Newtonian noise strain for breadboard, baffle, inner shield, outer shield, and cryostat, respectively, as shown in Fig. 10. Note that the displacement of TM due to breadboard/radiation shields and cryostat/baffle will be in opposite directions.

The breadboard NN dominates the entire 1–100 Hz spectra except for 21–23 Hz peaks where the radiation shields NN dominates because these are resonance mode of the shields. Even though the cryostat chamber is 10 times heavier than the radiation shield, its NN contribution is lower/comparable over the entire spectra due to symmetry and as it is further away from the TM. While, baffle is the closet object to the TM, its NN contribution is the lowest because of vibration attenuation from the baffle suspension and relatively low mass.

IV. IMPACT ON SENSITIVITY

Figure 11(a) shows the comparison of the cooling system NN with KAGRA design sensitivities and requirements.
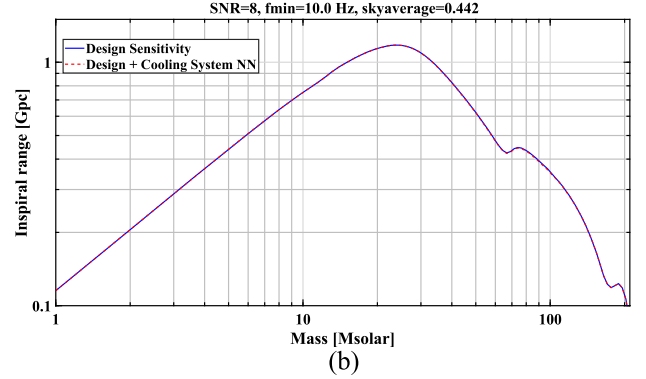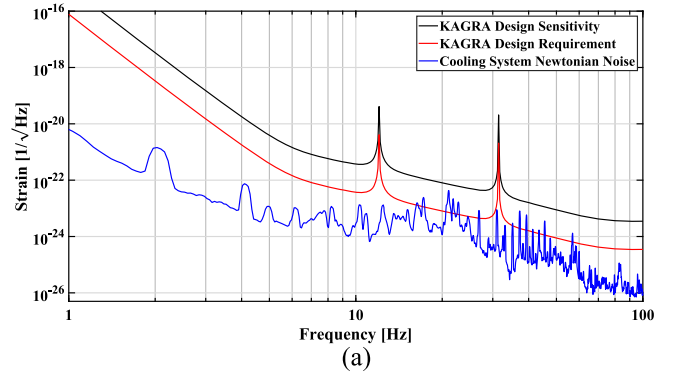

(a)

(b)

FIG. 11. (a) Comparison of KAGRA design sensitivity and requirement to cooling system Newtonian noise in 1–100 Hz bandwidth. Cooling system NN is below KAGRA design sensitivity but several peaks due cryocooler operation and structural resonances are larger than the requirement. Vibration source of these peaks and contributing component are summarized in Table II. (b) Comparison of KAGRA inspiral range with and without cooling system Newtonian noise. Note that the x-axis represents mass of a component object, assuming equal mass binaries.

Cooling system NN noise in Fig. 11(a) is denoted by blue spectra. NN coupling from the cooling system is lower than design sensitivity but there are several peaks between 16–50 Hz that are larger than the KAGRA design requirements. The vibration source and contributing component for this NN are summarized in Table II. The largest contribution comes from the breadboard except for 21.09 and 21.85 Hz peaks which are due to the shield resonance. Note that radiation shield contribution is based on the assumption that top and bottom half of shield moves with $u_{8K_{top}}$ and $u_{8K_{bottom}}$, respectively. We also evaluated the impact of cooling system NN on KAGRAs inspiral range, the results are plotted in Fig. 11(b). The inspiral range calculation was done using MATLAB code from [23] and assumes SNR of 8 and sky average of 0.442. Comparing the inspiral range of KAGRA with (red) and without (blue) cooling system NN, it is clear that this noise does not impact current KAGRA sensitivity. However, suppressing the cooling system Newtonian noise might be

TABLE II. Vibration source for cooling system NN peaks that exceed the KAGRA requirement in Fig. 11(a). The largest contribution comes from the breadboard except for the peaks marked "∗" which are due to radiation shield.

Vibration source	Frequency (Hz)
Chamber resonance	17.2, 21.8
Shield resonance	16.3, 21.1∗, 21.8∗
Cryocooler operation	26.8, 35.1, 37.2, 39.3, 41.3, 43.5, 45.5, 47.6, 46.9

essential in the future, when KAGRA sensitivity is improved [24], especially in low frequency. As Newtonian noise cannot be shielded against and reduction of vibration will require major design and infrastructure changes; two potential sequential solution are to first remove the breadboard since it has the largest contribution and then to subtract this noise from the interferometer data. The standard approach for NN subtraction is to generate Wiener filters using sensor arrays, several studies with this approach have shown promising results for seismic NN cancellation [25–27]. A similar approach using cryogenic accelerometers [22] should be explored and might be necessary for KAGRA in the future.

V. CONCLUSION

In this paper we present the estimation of Newtonian Noise coupling from the KAGRA cooling system in the 1–100 Hz bandwidth. First, a simple expression for NN coupling from a point mass/test mass system was derived, and this expression was then extended to the KAGRA cooling system by breaking each component into a mass distribution made up of multiple point masses. In order to simplify the calculations several considerations were made and the NN coupling for each component was evaluated.

Our calculations show that while the cooling system Newtonian noise is below KAGRA design sensitivity, several peaks above the KAGRA requirements exist in the 16–50 Hz band due to breadboard and radiation shields Newtonian noise coupling. The vibration sources for the NN were cryocooler operation and internal resonances of the chamber and radiation shield, making it difficult to attenuate this vibration (and corresponding NN peaks) without significant design and infrastructural changes.

While this noise does not limit the current detector sensitivity or inspiral range, it might be an issue in the future when KAGRA improves its sensitivity. Therefore, followup studies towards development of Wiener filters using cryogenic accelerometers to subtract cooling system Newtonian noise from KAGRA data are recommended. Furthermore, this study also shows that it will be important for the third-generation detectors to suppress the vibration of their cooling systems at design and infrastructural level.

VI. DATA AVAILABILITY

The data that support the findings of this study are available from the corresponding author upon reasonable request.

[1] Yoichi Aso, Yuta Michimura, Kentaro Somiya, Masaki Ando, Osamu Miyakawa, Takanori Sekiguchi, Daisuke Tatsumi, and Hiroaki Yamamoto, Interferometer design of the KAGRA gravitational wave detector, Phys. Rev. D **88**, 043007 (2013).

[2] T. Akutsu *et al.*, First cryogenic test operation of underground km-scale gravitational-wave observatory KAGRA, Classical Quantum Gravity **36**, 165008 (2019).

[3] J. Asai *et al.*, Advanced LIGO, Classical Quantum Gravity **32**, 074001 (2015).

[4] F. Acernese *et al.*, Advanced Virgo: A second-generation interferometric gravitational wave detector, Classical Quantum Gravity **32**, 024001 (2015).

[5] F. Matichard *et al.*, Seismic isolation of Advanced LIGO: Review of strategy, instrumentation and performance, Classical Quantum Gravity **32**, 185003 (2015).

[6] G. Ballardin, L. Bracci, S. Braccini, C. Bradaschia, C. Casciano, G. Calamai, R. Cavalieri, R. Cecchi, G. Cella, E. Cuoco *et al.*, Measurement of the VIRGO superattenuator

performance for seismic noise suppression, Rev. Sci. Instrum. **72,** 3643 (2001).

[7] P. R. Saulson, Terrestrial gravitational noise on a gravitational wave antenna, Phys. Rev. D **30,** 732 (1984).

[8] Teviet Creighton, Tumbleweeds and airborne gravitational noise sources for LIGO, Classical Quantum Gravity **25,** 125011 (2008).

[9] K. Pepper, Newtonian noise simulation and suppression for gravitational-wave interferometers, Technical Note T070192, LIGO, Pasadena, CA, 2007, https://dcc.ligo.org/LIGO-T070192/public.

[10] Donatella Fiorucci, Jan Harms, Matteo Barsuglia, Irene Fiori, and Federico Paolett, Impact of infrasound atmospheric noise on gravity detectors used for astrophysical and geophysical applications, Phys. Rev. D **97,** 062003 (2018).

[11] J. Harms, Terrestrial gravity fluctuations, Living Rev. Relativity **22,** 6 (2019).

[12] M. Punturo *et al.*, The Einstein telescope: A third-generation gravitational wave observatory, Classical Quantum Gravity **27,** 194002 (2010).

[13] D. Reitze, R. X. Adhikari, S. Ballmer, B. Barish, L. Barsotti, G. Billingsley, and M. Zucker, Cosmic explorer: The U.S. contribution to gravitational-wave astronomy beyond LIGO, Bull. Am. Astron. Soc. **51** (2019).

[14] Francesca Badaracco, Jan Harms, Camilla De Rossi, Irene Fiori, Kouseki Miyo, Taiki Tanaka, Takaaki Yokozawa, Federico Paoletti, and Tatsuki Washimi, KAGRA underground environment and lessons for the Einstein Telescope, Phys. Rev. D **104,** 042006 (2021).

[15] K. Somiya, Newtonian noise from the underground water (2019), http://www-kam2.icrr.u-tokyo.ac.jp/indico/event/3/session/32/contribution/365.

[16] C. Tokoku, N. Kimura, S. Koike *et al.*, Cryogenic system for the interferometric cryogenic gravitational wave telescope, KAGRA—design, fabrication, and performance test, AIP Conf. Proc. **1573,** 1254 (2014).

[17] R. Bajpai, T. Tomaru, N. Kimura, T. Ushiba, K. Yamamoto, T. Suzuki, and T. Honda, Vibration analysis of KAGRA cryostat at cryogenic temperature, Classical Quantum Gravity **39,** 165004 (2022).

[18] Edgard Bonilla, Brett Shapiro, Brian Lantz, Odylio Denys Aguiar, and Marcio Constancio, Noise requirements of the cryogenic shielding for next generation cryocooled gravitational wave observatories: Newtonian noise, Phys. Rev. D **104,** 122005 (2021).

[19] T. Ushiba *et al.*, Cryogenic suspension design for a kilometer-scale gravitational-wave detector, Classical Quantum Gravity **38,** 085013 (2021).

[20] Yoshiyuki Obuchi, Wide Angle Baffle desing review, Institute for Cosmic Ray Research, University of Tokyo Report No. JGW-G1706474-v1. (JGW Document Server).

[21] Simon Zeidler, Recent Activities of the AOS: WAB and NAB, Institute for Cosmic Ray Research, University of Tokyo Report No. JGW-G1808293-v1. (JGW Document Server).

[22] R. Bajpai, T. Tomaru, K. Yamamoto, T. Ushiba, N. Kimura, T. Suzuki, T. Yamada, and T. Honda, A laser interferometer accelerometer for vibration sensitive cryogenic experiments, Meas. Sci. Technol. **33,** 085902 (2022).

[23] Kentaro Komori, Latest estimated sensitivity of kagra (v201708), Institute for Cosmic Ray Research, University of Tokyo Report No. JGW-T1707038-v9. (JGW Document Server).

[24] Y. Michimura *et al.*, Prospects for improving the sensitivity of the cryogenic gravitational wave detector KAGRA, Phys. Rev. D **102,** 022008 (2020).

[25] G. Cella, Off-line subtraction of seismic newtonian noise, in *Recent Developments in General Relativity*, edited by B. Casciaro, D. Fortunato, M. Francaviglia, and A. Masiello (Springer, Milano, 2000), pp. 495–503, 10.1007/978-88-470-2113-6_44.

[26] Jennifer C. Driggers, Jan Harms, and Rana X. Adhikari, Subtraction of Newtonian noise using optimized sensor arrays, Phys. Rev. D **86,** 102001 (2012).

[27] Jan Harms, Krishna Venkateswara, Newtonian-noise cancellation in large-scale interferometric GW detectors using seismic tiltmeters, Classical Quantum Gravity **33,** 234001 (2016).